P7.1

HOW MIDLEVEL HORIZONTAL HUMIDITY GRADIENTS AFFECT SIMULATED STORM MORPHOLGY

Matthew J. Bunkers*
National Weather Service, Rapid City, South Dakota

1. INTRODUCTION

Of the many problems cloud models have, arguably a crucial one is the braking effect that realistic dry air has on modeled convective storms. Indeed, many have observed that cloud models often fail to produce sustained deep moist convection (DMC) with proximity soundings from severe storm environments that contain relatively dry air from above the level of free convection (LFC) through the midlevels. And in cases where DMC does develop, the storms usually are weaker than the ones in simulations without the dry air. For example, McCaul and Cohen (2004) and Beck and Weiss (2008) performed simulations with a variety of thermodynamic profiles, and showed that storms with realistic amounts of dry midlevel air were substantially reduced in size and intensity relative to their control cases. Moreover, Kirkpatrick et al. (2007) found that simulated updrafts failed to persist when the relative humidity (RH) was <60% above the LFC, and therefore initialized their model with the RH set to 90% above the LFC. They mentioned that model diffusion issues may be a concern with respect to storm demise, but pointed to entrainment of dry midlevel air as the primary limiting factor in updraft growth when the RH is low—according to the results of McCaul and Cohen (2004). Nevertheless, observations clearly indicate that strong, long-lived DMC occurs in the presence of dry midlevel air (e.g., Fig. 1; also see Fawbush and Miller 1954).

In contrast to above, others have been able to simulate convective storms in relatively dry midlevel environments. For example, Johnson et al. (1993) simulated a supercell storm from 2 August 1981 in southeastern Montana that had substantial ambient dry air from 700–300 mb, but they used a 3.5°C thermal perturbation to initiate convection. Likewise, Brooks et al. (1994), Gilmore and Wicker (1998), Bluestein (2000), and Bluestein and Weisman (2000) were able to simulate sustained DMC with relatively dry soundings of various depths and vertical placements, but they all used warm-rain (Kessler) microphysics and thermal perturbations that ranged from 1–1.5°C for Bluestein and Weisman (2000) to 4°C for Gilmore and Wicker (1998). Furthermore, Gilmore and Wicker observed that the updrafts and low-level mesocyclones weakened with time for cases with dry midlevels (centered at 750 mb in their study); vertical placement of the dry air was a factor in controlling the extent of this, with a higher placement being less detrimental.

* *Corresponding author address*: Dr. Matthew J. Bunkers, National Weather Service, 300 E. Signal Dr., Rapid City, SD 57701; e-mail: matthew.bunkers@noaa.gov

Recently, James and Markowski (2010) evaluated effects of dry air (centered at 700 mb) on simulated quasi-linear convective systems and supercells for CAPE of 1500, 3000, and 4500 J kg^{-1} (using a 3°C thermal perturbation). As with other studies, convective intensity for all simulations with dry air was reduced in terms of updraft mass flux and rainfall, and in addition the downdraft and cold pool strengths were reduced for the supercell simulations. The negative effects of the dry air were most pronounced for the low-CAPE environment because the entrainment rate is more sensitive to RH in this regime. James and Markowski demonstrated that the storms in the dry environments were not weaker because of excessive outflow; rather, they were weaker because of reduced buoyancy from entrainment (also see McCaul and Cohen 2004).

Kirkpatrick et al. (2007) and McCaul and Cohen (2004) further suggested that the real atmosphere must undergo some preconditioning whereby the RH is increased locally before DMC develops and is sustained [see Johnson and Mapes (2001) for a review]. For example, this can occur through low-level convergence which deepens and moistens the boundary layer (e.g., Wilson et al. 1992; Ziegler and Rasmussen 1998). Given a persistent forcing mechanism, repeated attempts of cumulus formation may eventually deepen and moisten the vertical column sufficiently to make the environment auspicious for DMC. When considering moistening of the boundary layer versus the midlevels, mobile sounding observations suggest that boundary layer moistening is most critical, and that the midlevels can remain rather dry (e.g., Bluestein et al. 1988; Ziegler et al. 2010).

If this preconditioning truly is required, perhaps the single initiating bubble is one reason why models often fail to sustain DMC in dry midlevel environments; one try simply is not enough in some cases. Even if the magnitude of the bubble is increased to the point where DMC is initiated, it may produce a storm that quickly grows too intense, and thus an outflow that outruns the updraft—leading to the storm's "premature" demise. Moreover, using too strong a perturbation is an unnatural way to initiate convection. Indeed, other more complicated methods, such as momentum or thermal flux techniques, have been able to produce sustained DMC when the single initiating bubble cannot (Loftus et al. 2008).

In light of this previous research, it remains unclear to what extent simulated convection is affected by variations in dry midlevel air. Is dry midlevel air always detrimental for DMC? Observations suggest not. Part of this problem stems from the inability of models to initiate and sustain DMC in dry midlevel air for a

reasonable amount of time. Applying warm-rain microphysics and/or excessive thermal perturbations is not the answer. In addition, simulations have not been conducted where storms started in moist air and then experienced dry midlevel air at a later time.

In order to better understand how simulated DMC responds to dry midlevel air—under the constraint of using a single initiating bubble with a realistic thermal perturbation—simulations of convective storms with simple horizontally inhomogeneous initial environments are conducted. Relatively little modeling work has been done in the area of cloud-scale to mesoscale inhomogeneous simulations, but some studies have started to address this issue (e.g., Skamarock et al. 1994; Atkins et al. 1999; Richardson et al. 2000, 2007; Houston and Niyogi 2007; Parker 2008; Ziegler et al. 2010; among others). Even so, no studies have addressed gradients of midlevel moisture. The present study thus takes a hybrid approach, somewhat akin to that of Ziegler et al. (2010), whereby dry midlevel air is gradually advected toward convection that is developing in a moist environment. This facilitates testing of the present hypothesis that if DMC can initiate prior to the arrival of dry midlevel air, it should have a better chance of surviving.

2. METHODS

All simulations herein were conducted using version 1.14 of the three-dimensional nonhydrostatic cloud model developed by Bryan and Fritch [2002, hereafter referred to as the Bryan Cloud Model (CM1)]. Relevant settings for CM1 are provided in Table 1 and Fig. 2.

The goal of this research necessitated CM1 to be initialized in a variety of ways. First, the familiar Weisman and Klemp (1982, hereafter WK82) thermodynamic profile was used as the control "moist" homogeneous environment (Fig. 3a). A unidirectional wind profile was employed in order to keep the inhomogeneous experiments simple. The wind varied uniformly by 25 m s^{-1} (49 kt) over the lowest 6 km AGL, and was constant from 6–20 km. The 0–6-km shear was 0.004 s^{-1}, which when combined with a mixed-layer CAPE (MLCAPE) of 2079 J kg^{-1}, resulted in a bulk Richardson number (BRN) of 46, which is supportive of supercellular convection.

The other homogeneous environment consisted of the WK82 sounding that had arbitrary drying applied to the 800–250-mb layer, with peak reductions in RH near 600 mb (51% drier) and 400 mb (56% drier) (Fig. 3b, hereafter dry0). [The bottom dry layer is nearest to Gilmore and Wicker's (1998) higher-altitude placement.] The MLCAPE was slightly higher (2141 J kg^{-1}), resulting in a BRN of 47. Dry0 was based on operational experience of observed drying in soundings due to (1) advection of the elevated mixed layer over the central United States and (2) upper-level drying associated with jet streaks. The dry layers in Fig. 3b also loosely correspond to those in the 0000 UTC 24 June 2002 sounding from Aberdeen, South Dakota, which was associated with an F4-producing tornadic supercell. Indeed, this case provided some of the motivation for the present study because of the difficulties in modeling convection when starting from this base state.

The main part of this study consists of four simple inhomogeneous experiments in which the horizontal placement of the dry midlevel air was altered to simulate the effects of dry air arriving—from the west—at varying times (Table 2; Fig. 2). After testing various configurations, a total of 11 additional soundings were constructed that varied linearly from dry0 (Fig. 3b) to WK82 (Fig. 3a). The eastern one-half to two-thirds of the domain consisted of the WK82 sounding and the extreme western part of the domain consisted of the dry0 sounding; the intermediate part of the domain had the same temperature profile but with the 11 soundings containing progressively drier midlevels from east to west. These experiments allowed dry air to arrive relatively quickly (e.g., dry1, Fig. 2a), as well as after DMC was well underway (dry4, Fig. 2d). Thus, the horizontal humidity gradient was held constant for these four experiments; only the timing was changed.

Thirteen soundings were used because that was sufficient to minimize artificial vertical motion in the model that occurred because of the imposed horizontal moisture gradient. For example, in the dry3 experiment without a triggering mechanism, perturbations were mostly <10 cm s^{-1} and confined to a relatively small part of the domain (Fig. 4a). However, for a test experiment similar to dry3—but using only the dry0 and WK82 soundings and thus a much larger gradient of horizontal humidity—the perturbations had absolute magnitudes in excess of 50 cm s^{-1} and occurred over a much larger area (Fig. 4b). Interestingly, the simulated reflectivity at 180 min was not that different between these two runs (when using a triggering mechanism), except for a somewhat smaller and weaker storm in the two-sounding simulation (not shown).

Convection was initiated with a thermal perturbation of magnitude 1 °C at the center of the domain (Table 1; Fig. 2). A constant zonal grid translation speed of –2 m s^{-1} was applied in all experiments so the simulated storms would remain near the center of the domain. Although the perturbation could have been placed in the eastern part of the domain with a relatively large translation speed toward the east—thus allowing for even greater variability in the timing of the midlevel drying—it was desired to have a minimal translation speed because simulation differences were noted when the domain translation speed was varied (also see Brooks et al. 1994).

Three different ice microphysics variations were utilized herein (Table 1) given the sensitivity of cloud model simulations to this particular parameterization (Straka and Rasmussen 1998), as well as the general lack of knowledge of microphysical characteristics of DMC. The widely used Lin et al. (1983) single-moment scheme, as modified by Tao and Simpson (1989), was employed in two different ways. The first option (hereafter LFOA) adopted the widely used intercept parameter for rain (8.0×10^6 m^{-4}) and a slightly smaller than usual intercept parameter for hail (2.0×10^4 m^{-4})—also known as the high-density precipitating ice category. These are the default settings in CM1. The second option (hereafter LFOB) used a notably reduced

intercept parameter for rain (0.4×10^6 m^{-4}) and the more traditional intercept parameter for hail [4.0×10^4 m^{-4}; as prescribed by Lin et al. (1983)]. LFOA can be considered a "standard" raindrop scheme and LFOB can be considered a "large" raindrop scheme (e.g., Snook and Xue 2008). Dawson et al. (2010) found that the LFOB settings (referred to as LINB in their study) produced results similar to their double- and triple-moment schemes for the particular case they were examining. The third microphysics option is that of Thompson et al. (2008, hereafter Thompson). This is a double-moment scheme for ice crystals and rain (rain was added to CM1 in 2009); otherwise it is a single-moment scheme for the remaining hydrometeors. Output from the microphysics schemes were used to derive simulated reflectivity (e.g., Smith et al. 1975; Kain et al. 2008) to help with the interpretation of model output.

3. RESULTS

3.1 Simple Inhomogeneous Experiments

All of the results focus mainly on the right half of the domain and ignore the left because of the unidirectional shear profile which leads to north–south symmetry centered at y = 60 km. The homogeneous simulation using the WK82 sounding and LFOA microphysics produced a high precipitation (HP)-type supercell on the southern end of a line of storms at 180 min (Fig. 5a). In contrast to this, the homogeneous simulation using the dry0 sounding resulted in an isolated and much smaller supercell at 180 min (Fig. 5b); this storm struggled in the presence of homogeneous dry midlevel air. These results are consistent with McCaul and Cohen (2004) and James and Markowski (2010) in that the dry air resulted in an overall reduction of hydrometeors, as well as smaller convective cells.

The dry0 experiment was repeated with initial perturbations of 2–4°C for the LFOA microphysics, consistent with previous studies in which progressively larger thermal perturbations were used as the midlevel RH decreased (e.g., McCaul and Cohen 2004). The storm completely dissipated by 180 min for the 2°C bubble, although it did develop faster than the WK82 storm. However, for the 3°C bubble the storm persisted through 180 min, although it was weaker than for the 1°C case, and also was associated with a weak line of broken convection to its north (not shown). Interestingly, the storm for the 4°C bubble almost dissipated by 150 min, but the intervening broken convection was still prevalent like in the 3°C case. Stronger cold pools are believed to be the reason for the earlier demise and more linear nature of the storms with 2–4°C perturbations (relative to the dry0 run).

Strong, isolated supercells were sustained through 180 min in the dry2–dry4 inhomogeneous runs for the LFOA microphysics (Figs. 5d–f). These three storms appeared similar when using the 2–5-km updraft helicity (UH, Kain et al. 2008) to quantify supercell strength. A low-precipitation-type supercell was apparent for the dry1 case (Fig. 5c), which structurally appears closest to the dry0 case (Fig. 5b). This is expected because the dry midlevel air arrived almost immediately in the dry1 simulation (Table 2), making it most similar to the dry0 scenario. Surprisingly, the UH was greatest for dry0, and lowest for WK82, suggesting that even for small storms, the combination of low-level vorticity and vertical motion still can be quite substantial.

The results for the LFOB microphysics generally mirror those for LFOA, with a few exceptions (cf. Figs. 5 and 6). First, instead of a relatively weak and HP-type supercell for the WK82 simulation, a large and strong classic supercell was produced (Fig. 6a). Second, the storm for the dry0 run had all but dissipated by 180 min (Fig. 6b). Otherwise, the storms were progressively larger and generally stronger from dry1–dry4, with a similar southward deviation for WK82 and dry4.

Relatively more hydrometeors were produced for the Thompson microphysics scheme compared to the two LFO variants (Fig. 7), but the overall trends were similar. The main points to take from this set of simulations are the following: (1) the WK82 run produced an HP/bow echo type mode by 180 min; (2) storms for dry0 and dry1 were similar to each as was the case for the two LFO variants; and (3) storms were progressively stronger in terms of UH for the dry2–dry4 runs, even though the most well defined and isolated supercell occurred for the dry3 run.

The domain maximum vertical velocity (w_{max}) was similar among the WK82, dry3, and dry4 simulations for all respective runs (Fig. 8). This implies an undiluted ascent (or at least minimum dilution) in the updraft cores for storms even when dry air was present (e.g., McCaul and Cohen 2004; James and Markowski 2010). Conversely, w_{max} was substantially reduced in the dry0 and dry1 simulations for all cases (Fig. 8, solid green and blue lines). The greatest variability of w_{max} among the three sets of microphysics experiments was for the dry2 run (Fig. 8, cf. dashed red lines); recall this experiment had dry midlevel air starting to arrive at the center of the domain by 20 min into the simulation. The LFOA microphysics scheme for dry2 was able to maintain a steadier storm and w_{max}, but the dry2 w_{max} for the LFOB and Thompson microphysics schemes was much more variable and weaker for the last half of the simulations.

In order to further quantify the supercells for the LFOA microphysics scheme, time series of the maximum UH for the WK82 and dry2–dry4 runs were created. The first peak in UH occurred at 30 min for all four cases as the storms were splitting (Fig. 9). The UH then increased between 40–50 min, but this increase was most pronounced for the WK82 run and least pronounced for the dry2 run. The trends in UH during this time clearly appear to be related to the timing of the dry midlevel air. Interestingly, the UH for the dry2–dry4 runs increased markedly between 70–80 min (Fig. 9), but remained steady for the WK82 run. Additional increases and decreases in UH occurred throughout the remainder of the simulation, with comparable values among the four runs. Moreover, the mean UH was 57-77 m^2 s^{-2} greater for the dry2–dry4 runs versus WK82. This trend of "retarded growth" after the arrival of dry midlevel air, and then further storm re-intensification,

also was evident for the LFOB and Thompson microphysics cases.

Summarizing the results from these three sets of experiments, it is evident that the nature and intensity of the supercells in some of the inhomogeneous runs is comparable to that for the corresponding moist homogeneous control run. Although the dry midlevel air may at first appear inimical to the simulated storms, the storms can indeed survive, intensify, and maintain substantial rotation after encountering the dry midlevel air (assuming the dry air doesn't arrive too soon, as in dry1). In fact, it is argued that the supercells are even stronger and/or better organized for some of the inhomogeneous LFOA and Thompson microphysics cases (versus the WK82 runs). Even though the dry midlevel air reduces the size of the storms as well as the amount of liquid water content, it also is more likely to produce relatively isolated supercells, thus replicating radar observations of actual storms in dry midlevel environments (Fig. 1). Thus, preconditioning the cloud model with a moist sounding—prior to the arrival of dry midlevel air—promotes storm longevity and intensity.

3.2 Sensitivity Tests

It is apparent that the convective mode is sensitive to the microphysics schemes, as indicated in Figs. 5–7 (also see Snook and Xue 2008). This suggests there may be other nontrivial sensitivity of the results to various model settings (e.g., Straka and Rasmussen 1998). Hence, additional sensitivity tests were conducted to assess the applicability of the results to other regimes and temporal scales.

a) Reverse simulation of dry4

In the first sensitivity test, a simulation was carried out for which the horizontal moisture gradient in dry4 was reversed (Table 2). Thus, the storm was initiated in the dry0 environment, but moist midlevel air began to arrive by 40 min. By 120 min the WK82 moisture profile had reached the western extent of storm. In effect, this tested the relative importance of having a moist environment prior to and during initiation *versus* a moist environment after initiation.

The storms that began in the moist environment (dry4) clearly had an advantage over the storms that started in the dry midlevel environment (reverse-dry4) for the LFOA and Thompson microphysics schemes (Fig. 10). Not only were the supercells larger and stronger for the dry4 experiment, but they had deviated about 15 km further south by 180 min (Figs. 10a, b, e, and f). In the case of the LFOB microphysics, the supercell was relatively small prior to 150 min for the reverse-dry4 case, but thereafter had a size similar to that of the dry4 case. Nevertheless, the supercell for the LFOB dry4 case had deviated about 8 km further south by 180 min (Figs. 10c and d), and had a larger updraft and more "classic" looking appearance (even though the UH was larger for the LFOB reverse-dry4 case). Therefore, storms that started in moist air, but then experienced dry midlevel air, were consistently as strong, if not stronger, than the reverse scenario.

b) Red Rock, Oklahoma, 26 April 1991

The 0000 UTC 27 April 1991 sounding from Norman, Oklahoma—associated with an F4-producing tornadic supercell near Red Rock—was another impetus for performing the present study. This "Red Rock" sounding had a deep moist layer up to 700 mb, but then considerable drying was evident from 672–400 mb (RH = 6–21%). When running CM1 with the observed Red Rock sounding and a 1°C bubble, only a brief 25–40 dBZ echo was produced for all three microphysics schemes. However, using a 2–3°C bubble did initiate DMC which persisted through 180 min.

In order to test this case further, the observed Red Rock sounding was modified such that the RH was 80% above the LFC; otherwise, the temperature and wind profile remained unaltered. When running CM1 for this case, large and strong classic supercells were produced (Figs. 11b, d, and f). Next, the dry3 experiment was setup as in Fig. 2c, but instead varied from the observed Red Rock sounding on the west to the "moist" Red Rock sounding on the east. This set of experiments also resulted in large and strong supercells that, in addition, were relatively more isolated than for the "moist" Red Rock case (Figs. 11a, c, and e). Furthermore, values of UH for the various microphysics schemes indicate that (1) the storms were similar in strength for LFOA (Figs. 11a and b); (2) the storm was weaker for dry3-LFOB (Figs. 11c and d); and (3) the storm was stronger for dry3-Thompson (Figs. 11e and f). Thus, although the observed Red Rock sounding failed to produce DMC with the 1°C bubble, when initialized with a "moist" sounding followed by advection of the observed Red Rock sounding with dry midlevel air, strong supercells were sustained in the model.

c) 4-hr simulations and grid translation

The third sensitivity test was conducted primarily to determine if storms in the dry midlevel air would persist even longer than 180 min. Thus, the WK82 and dry3 experiments were repeated for durations of 240 min (4 hr), which required a small change in the meridional grid translation speed to keep the right-moving storms within the domain.

Despite the continued presence of dry midlevel air after 180 min, supercells were maintained through 240 min for the LFOA and LFOB runs, and they remained as strong at 240 min as they were at 180 min. The supercell for the Thompson run, however, evolved into a bow echo by 230 min hr, but it still was a strong supercell from 180–220 min. Overall the basic results for the 3-hr runs were confirmed by the 4-hr runs; long-lasting supercells were observed in all cases.

Another interesting result is that simply changing the grid translation speed altered the number of storms and general morphological features at 180 min. At any rate, the convective mode remained the same at 180 min between the 3-hr runs (first part of section 3) and 4-hr runs for all three microphysics options. Thus, one should use caution when comparing the details from simulations that have differing grid translation speeds.

d) Grid spacing

Bryan et al. (2003) recommended grid spacing on the order of 100 m for most research applications—based on a turbulence perspective—but also noted that on the order of 1000 m was acceptable for the operational community. The grid spacing of 1000 m in the present study is therefore inadequate to resolve specific details of the convection; however, it was a constraint based on the available computational power.

To examine this, additional runs for the WK82 and dry3 experiments were performed with horizontal grid spacing of $\Delta x = \Delta y = 500$ m, along with smooth vertical stretching from $\Delta z = 100$ m at 3km to $\Delta z = 500$ m at 9 km (constant above and below). Considerable differences in the simulation details were evident for the two different grid lengths, but the overall patterns were quite similar at 180 min when using the LFOA and LFOB microphysics. The main exception is for the LFOA dry3 experiment, in which considerably more convection was present for the simulation with smaller grid spacing. In contrast, the Thompson scheme resulted in less convection for both WK82 and dry3 when using smaller grid spacing, with a tendency for differences in convective mode. Although not tested, some of the differences arising from grid translation (section 3.2c) may be dependent on the grid spacing.

4. DISCUSSION

The first noteworthy finding from this study is that simulated convective storms can survive and intensify in dry midlevel air when using a modest thermal perturbation if the model is "preconditioned" with a moist sounding. The dry1–dry4 simple inhomogeneous experiments strongly support this because the dry1 experiment produced storms that looked more like those from the homogeneous dry0 run, whereas the dry3–dry4 runs produced supercells consistent with the WK82 homogeneous control run; timing of the drying clearly is important. The reverse-dry4 experiment adds more support to this argument because the storms in this set of simulations really struggled in the first 90–120 min of their lifetimes. Only the LFOB case was able to gain appreciably intensity, which appeared to be because of the "large" raindrops and weaker initial cold pool that did not outrun the storm prior to the arrival of the moist midlevel air. Because the initiating mechanism is so strongly implicated in this research, additional experiments using a thermal or momentum flux method, as in Loftus et al. (2008), should help elucidate the importance of preconditioning.

A second interesting result is the potential effect dry midlevel air has on convective mode—namely, to be more likely to produce an isolated, strong, and long-lived storm, which is congruent with radar observations. This apparent enhancement of simulated storms may be partly related to the lack of interference from neighboring cells. James and Markowski (2010) found that dry (versus moist) midlevel air favors less hydrometeors and a weaker cold pool in simulated DMC, consistent with the present study. This implies less interference between nearby cells because their cold pools should not be as destructive to one another. This also implies there would be fewer strong cells as the weaker ones are desiccated by the dry midlevel air. Moreover, results indicate w_{max} is not reduced in some simulations with dry midlevel air, thus the storms that do survive can be at least as intense as their more numerous and often times larger counterparts.

Relatively little has been done to study observations of convective mode paired with midlevel moisture. Dial and Racy (2004) evaluated low-level RH (below 700 mb) with respect to convective mode, but found it did not discriminate between discrete and linear evolutions. Conversely, Doswell and Evans (2003) examined the environments of derechos and supercells and found that soundings associated with significant tornadoes had high boundary layer RH, but they also had the lowest 700–500-mb mean RH out of all the other supercell and derecho classes. Furthermore, the 700–500-mb mean RH was highest for their three derecho categories (linear mode). These results agree with the present study insofar as the moist midlevel environments tended to favor a linear convective mode and the dry midlevel environments favored a discrete convective mode.

5. CONCLUSION

This study bridges some of the gap in understanding between the observed and modeled effects of dry midlevel air on DMC; dry air is not always harmful. Nevertheless, additional work is needed to more fully understand the sensitivity of simulated convective storms to variations in midlevel moisture gradients, and to what extent dry midlevel air is detrimental to the initiation and maintenance of DMC. Perhaps most importantly the grid spacing used herein should be refined such that turbulence can be adequately addressed. Other items to be considered are different (1) horizontal gradients of dry air, (2) vertical placements of dry air, (3) magnitudes of dry air, (4) times for when the dry air arrives, and (5) configurations for the reverse experiment. With regard to vertical placements of the dry air, the Aberdeen sounding referenced in section 2 has notably lower RH in the boundary layer compared to the Red Rock sounding, which has made it difficult to use in model simulations [also see Bluestein and Weisman (2000) for effects of dry low-level air on DMC]. Therefore, the relative sensitivity of low-level versus midlevel dry air could be explored with a combination of these soundings.

Acknowledgments. I am indebted to Paul Markowski for getting me started with George Bryan's cloud model, and to George Bryan for making his model freely available. Discussions with Andy Detwiler, Dick Farley, Mark Hjelmfelt, Jennifer Laflin, Dave Schultz, Paul Smith, Tom Warner, and Jon Zeitler helped improve this research. The technical support provided by Eric Helgeson, Greg Mann, and Kelly Whitaker also is appreciated. All model graphics were produced with the Grid Analysis and Display System (GrADS). Finally, I thank Dave Carpenter (Meteorologist-in-Charge, NWS Rapid City, SD) for supporting this work.

REFERENCES

Atkins, N. T., M. L. Weisman, and L. J. Wicker, 1999: The influence of preexisting boundaries on supercell evolution. *Mon. Wea. Rev.*, **127**, 2910–2927.

Beck, J., and C. Weiss, 2008: The effects of thermodynamic variability on low-level baroclinity and vorticity within numerically simulated supercell thunderstorms. Preprints, *24th Conf. on Severe Local Storms,* Savannah, GA, Amer. Meteor. Soc., P3.17. [Available online at http://ams.confex.com/ams/pdfpapers/141926.pdf.]

Bluestein, H. B., 2000: A tornadic supercell over elevated, complex terrain: The Divide, Colorado, storm of 12 July 1996. *Mon. Wea. Rev.,* **128,** 795–809.

____, and M. L. Weisman, 2000: The interaction of numerically simulated supercells initiated along lines. *Mon. Wea. Rev.*, **128**, 3128–3149.

____, E. W. McCaul Jr., G. P. Byrd, and G. R. Woodall, 1988: Mobile sounding observations of a tornadic storm near the dryline: The Canadian, Texas storm of 7 May 1986. *Mon. Wea. Rev.,* **116,** 1790–1804.

Brooks, H. E., C. A. Doswell III, and R. B. Wilhelmson, 1994: The role of midtropospheric winds in the evolution and maintenance of low-level mesocyclones. *Mon. Wea. Rev*., **122**, 126–136.

Bryan, G. H., and J. M. Fritsch, 2002: A benchmark simulation for moist nonhydrostatic numerical models. *Mon. Wea. Rev.,* **130,** 2917–2928.

____, J. C. Wyngaard, and J. M. Fritsch, 2003: Resolution requirements for the simulation of deep moist convection. *Mon. Wea. Rev.,* **131,** 2394–2416.

Dawson, D. T., II, M. Xue, J. A. Milbrandt, and M. K. Yau, 2010: Comparison of evaporation and cold pool development between single-moment and multimoment bulk microphysics schemes in idealized simulations of tornadic thunderstorms. *Mon. Wea. Review,* **138,** 1152–1171.

Dial, G. L., and J. P. Racy, 2004: Forecasting short term convective mode and evolution for severe storms initiated along synoptic boundaries. Preprints, *22nd Conf. on Severe Local Storms*, Hyannis, MA, Amer. Meteor. Soc., 11A.2. [Available online at http://ams.confex.com/ams/pdfpapers/81495.pdf.]

Doswell, C. A., III, and J. S. Evans, 2003: Proximity sounding analysis for derechos and supercells: An assessment of similarities and differences. *Atmos. Res.,* **67,** 117–133.

Durran, D. R., and J. B. Klemp 1983: A compressible model for the simulation of moist mountain waves. *Mon. Wea. Rev.,* **111,** 2341–2361.

Fawbush, E. J., and R. C. Miller, 1954: The types of airmasses in which North American tornadoes form. *Bull. Amer. Meteor. Soc*., **35**, 154–165.

Gilmore, M. S., and L. J. Wicker, 1998: The influence of midtropospheric dryness on supercell morphology and evolution. *Mon. Wea. Rev.*, **126**, 943–958.

Houston, A. L., and D. Niyogi, 2007: The sensitivity of convective initiation to the lapse rate of the active cloud-bearing layer. *Mon. Wea. Rev.,* **135,** 3013–3032.

James, R. P., and P. M., Markowski, 2010: A numerical investigation of the effects of dry air aloft on deep convection. *Mon. Wea. Rev.*, **138**, 140–161.

Johnson, D. E., P. K. Wang, and J. M. Straka, 1993: Numerical simulations of the 2 August 1981 CCOPE supercell storm with and without ice microphysics. *J. Appl. Meteor.* **32,** 745–759.

Johnson, R. H., and B. E. Mapes, 2001: Mesoscale processes and severe convective weather. *Severe Convective Storms, Meteor. Monogr.,* No. 50, Amer. Meteor. Soc., 71–122.

Kain J. S., and Coauthors, 2008: Some practical considerations regarding horizontal resolution in the first generation of operational convection-allowing NWP. *Wea. Forecasting,* **23,** 931–952.

Kirkpatrick, J. C., E. W. McCaul Jr., and C. Cohen, 2007: The motion of simulated convective storms as a function of basic environmental parameters. *Mon. Wea. Rev.,* **135,** 3033–3051.

Klemp, J. B., and R. B. Wilhelmson, 1978: The simulation of three-dimensional convective storm dynamics. *J. Atmos. Sci.*, **35**, 1070–1096.

Lin, Y.-L., R. D. Farley, and H. D. Orville, 1983: Bulk parameterization of the snow field in a cloud model. *J. Climate Appl. Meteor.*, **22**, 1065–1092.

Loftus, A. M., D. B. Weber, and C. A. Doswell III, 2008: Parameterized mesoscale forcing mechanisms for initiating numerically simulated isolated multicellular convection. *Mon. Wea. Rev.,* **136,** 2408–2421.

McCaul, E. W., Jr., and C. Cohen, 2004: The initiation, longevity and morphology of simulated convective storms as a function of free tropospheric relative humidity. Preprints, *22nd Conf. on Severe Local Storms*, Hyannis, MA, Amer. Meteor. Soc., 8A.5. [Available online at http://ams.confex.com/ams/pdfpapers/81251.pdf.]

Parker, M. D., 2008: Response of simulated squall lines to low-level cooling. *J. Atmos. Sci.,* **65,** 1323–1341.

Richardson, Y. P., K. Droegemeier, and R. Davies-Jones, 2000: The influence of horizontal variations in vertical shear and low-level moisture on numerically simulated convective storms. Preprints*, 20th Conf. on Severe Local Storms*, Orlando, FL, Amer. Meteor. Soc., 599–602.

____, ____, and ____, 2007: The influence of horizontal environmental variability on numerically simulated convective storms. Part I: Variations in vertical shear. *Mon. Wea. Rev.,* **135,** 3429–3455.

Skamarock, W. C., M. L. Weisman, C. A. Davis, and J. B. Klemp, 1994: The evolution of simulated mesoscale convective systems in idealized environments. Preprints*, Sixth Conf. on Mesoscale Processes*, Portland, OR, Amer. Meteor. Soc., 407–410.

Smith, P. L., Jr., C. G. Myers, and H. D. Orville, 1975: Radar reflectivity factor calculations in numerical cloud models using bulk parameterization of precipitation. *J. Appl. Meteor.,* **14,** 1156–1165.

Snook, N., and M. Xue, 2008: Effects of microphysical drop size distribution on tornadogenesis in supercell thunderstorms. *Geophys. Res. Lett.*, **35,** L24803.

Straka, J. M., and E. N. Rasmussen, 1998: Thirty years of cloud modeling: Does the emperor wear clothes? Preprints*, 19th Conf. on Severe Local Storms*, Minneapolis, MN, Amer. Meteor. Soc., 342–347.

Tao, W.-K., and J. Simpson, 1989: Modeling study of a tropical squall-type convective line. *J. Atmos. Sci.,* **46,** 177–202.

Thompson, G., P. R. Field, R. M. Rasmussen, and W. D. Hall, 2008: Explicit forecasts of winter precipitation using an improved bulk microphysics scheme. Part II: Implementation of a new snow parameterization. *Mon. Wea. Rev.,* **136,** 5095–5115.

Weisman, M. L., and J. B. Klemp, 1982: The dependence of numerically simulated convective storms on vertical wind shear and buoyancy. *Mon. Wea. Rev.*, **110**, 504–520.

Wilson, J. W., and Coauthors, 1992: The role of boundary-layer convergence zones and horizontal rolls in the initiation of thunderstorms: A case study. *Mon. Wea. Rev.,* **120,** 1785–1815.

Ziegler, C. L., and E. N. Rasmussen, 1998: The initiation of moist convection at the dryline: Forecasting issues from a case study perspective. *Wea. Forecasting,* **13,** 1106–1131.

____, E. R. Mansell, J. M. Straka, D. R. MacGorman, and D. W. Burgess, 2010: The impact of spatial variations of low-level stability on the life cycle of a simulated supercell storm. *Mon. Wea. Rev.,* **138,** 1738–1776.

TABLES AND FIGURES

Table 1. Settings for the Bryan Cloud Model (CM1) version 1.14 used in the present study.

domain	120 x 120 x 20 km
Δx, Δy	1000 m
Δz	500 m
large time step	6 sec
small time step	0.75 sec
simulation time	180 min
output frequency	10 min
initiating bubble	1°C at center of domain; h = 1400 m; r_z = 1400 m; $r_{x\text{-}y}$ = 10 km
microphysics (3 options**)**	NASA Goddard versions of Lin et al. (1983) as follows: LFOA → $N_{0r} = 8.0 \times 10^6$ m^{-4}; $N_{0h} = 2.0 \times 10^4$ m^{-4}; ρ_h = 900 kg m^{-3} LFOB → $N_{0r} = 0.4 \times 10^6$ m^{-4}; $N_{0h} = 4.0 \times 10^4$ m^{-4}; ρ_h = 900 kg m^{-3} Thompson et al. (2008), 2-moment ice crystals and rain
Coriolis	off
radiation	off
surface fluxes	zero
top/bottom boundaries	free slip
lateral boundaries	open radiative (Durran and Klemp 1983)
Raleigh damping layer	15–20 km
pressure solver	time-splitting, fully explicit (Klemp and Wilhelmson 1978)
advection scheme	5th order
diffusion scheme	6th order

Table 2. Experiment nomenclature for the various CM1 initializations (refer to section 2 for more details).

a) WK82	horizontally homogeneous with WK82 profile (Fig. 3a)
b) dry0	horizontally homogeneous with "dry" version of WK82 profile (Fig. 3b)
c) dry1	simple inhomogeneous with dry air advection by 10 min into the simulation
d) dry2	simple inhomogeneous with dry air advection by 20 min into the simulation
e) dry3	simple inhomogeneous with dry air advection by 30 min into the simulation
f) dry4	simple inhomogeneous with dry air advection by 40 min into the simulation
h) reverse-dry4	simple inhomogeneous with moist air advection by 40 min into the simulation (i.e., same as dry4 but the moisture gradient was reversed)

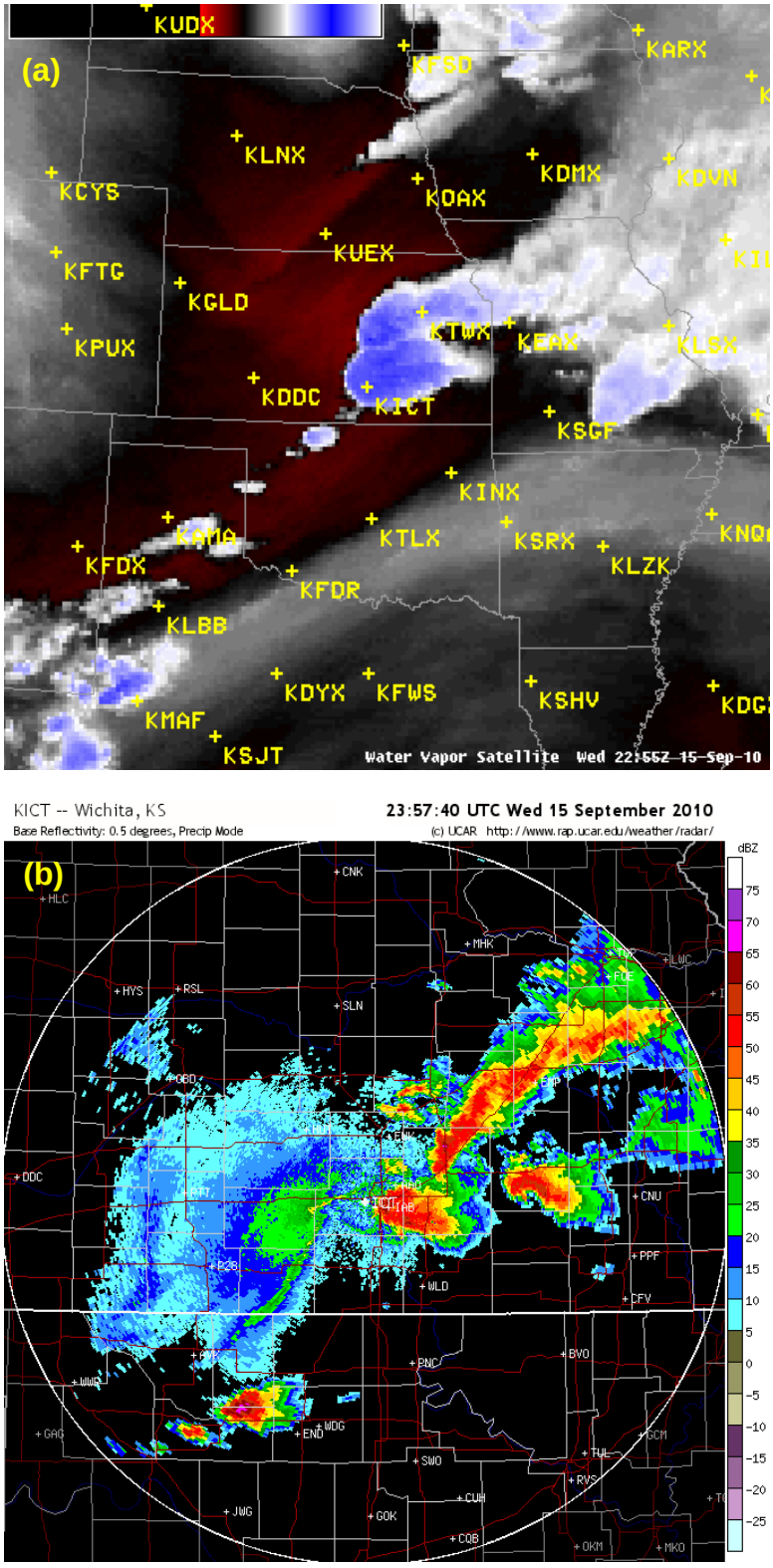

Figure 1. (a) Water vapor (6.7 μm) image valid at 2255 UTC 15 September 2010 over the central United States and (b) 0.5° base reflectivity radar image from Wichita, KS (KICT, center of image) valid 63 min later at 2358 UTC. Three supercells, to the southwest through east of KICT, had intensified from 2255–2358 UTC in the presence of the ambient dry midlevel air, while a line of storms persisted to the northeast of KICT.

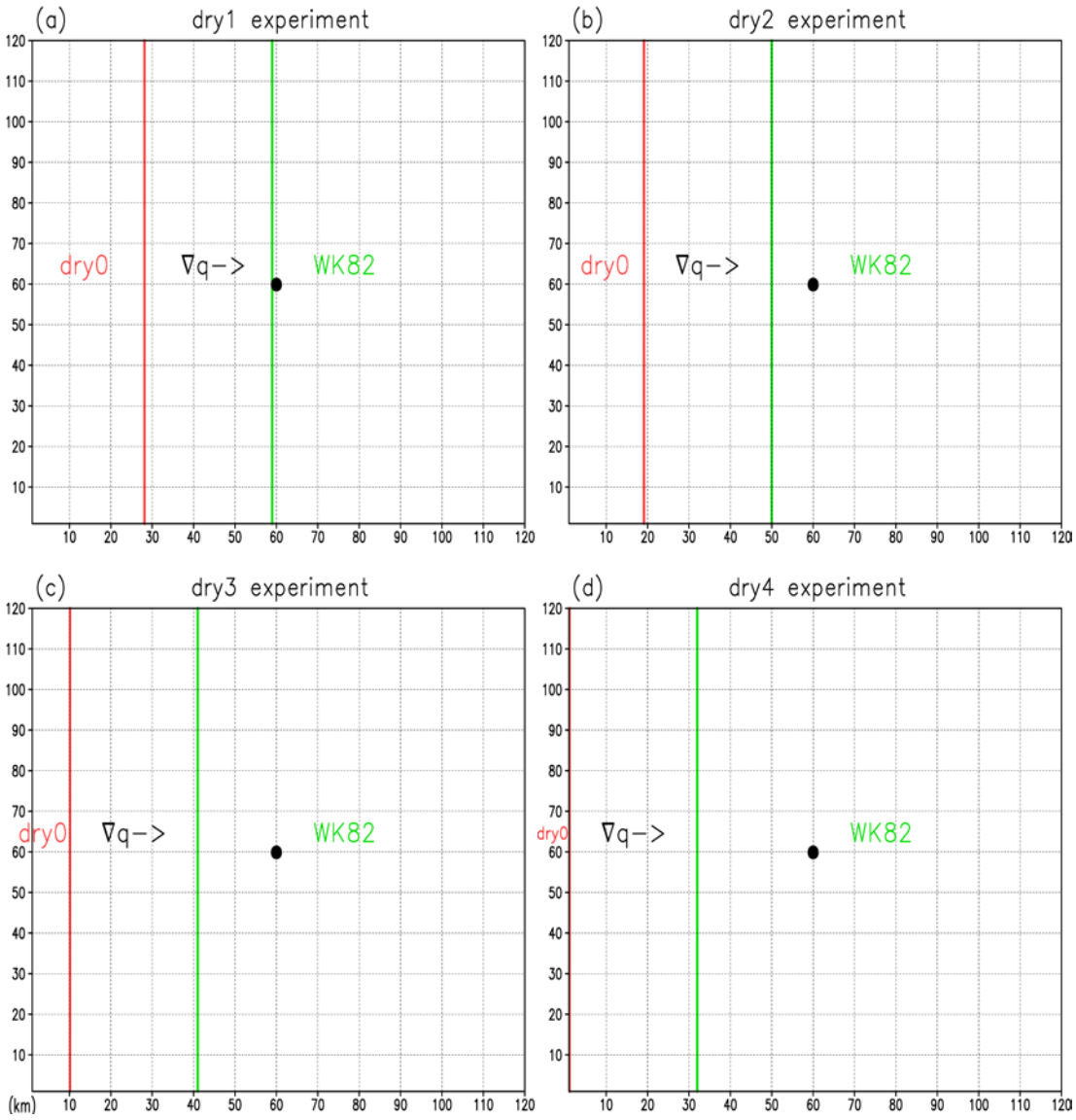

Figure 2. Horizontal domain (km) for the cloud model simulations, as well as the setup for the four primary inhomogeneous experiments. In these four cases, the area to the east of the green line was initialized with the "WK82" sounding (Fig. 3a); the area to the west of the red line was initialized with the "dry0" sounding (Fig. 3b), and the area between the red and green lines was initialized by linearly interpolating between dry0 and WK82 (resulting in 11 interpolated soundings). [Note that in (d) the dry0 sounding was placed along the westernmost column of grid boxes.] The horizontal gradient of moisture is represented by "$\nabla q->$" and the black dot at x = 60, y = 60, is the location of the 1 °C bubble. A fifth inhomogeneous experiment, reverse-dry4, was conducted that used the same setup as (d), except the moisture gradient was reversed—thus allowing the storm to start in dry midlevel air followed by the advection of moist midlevel air.

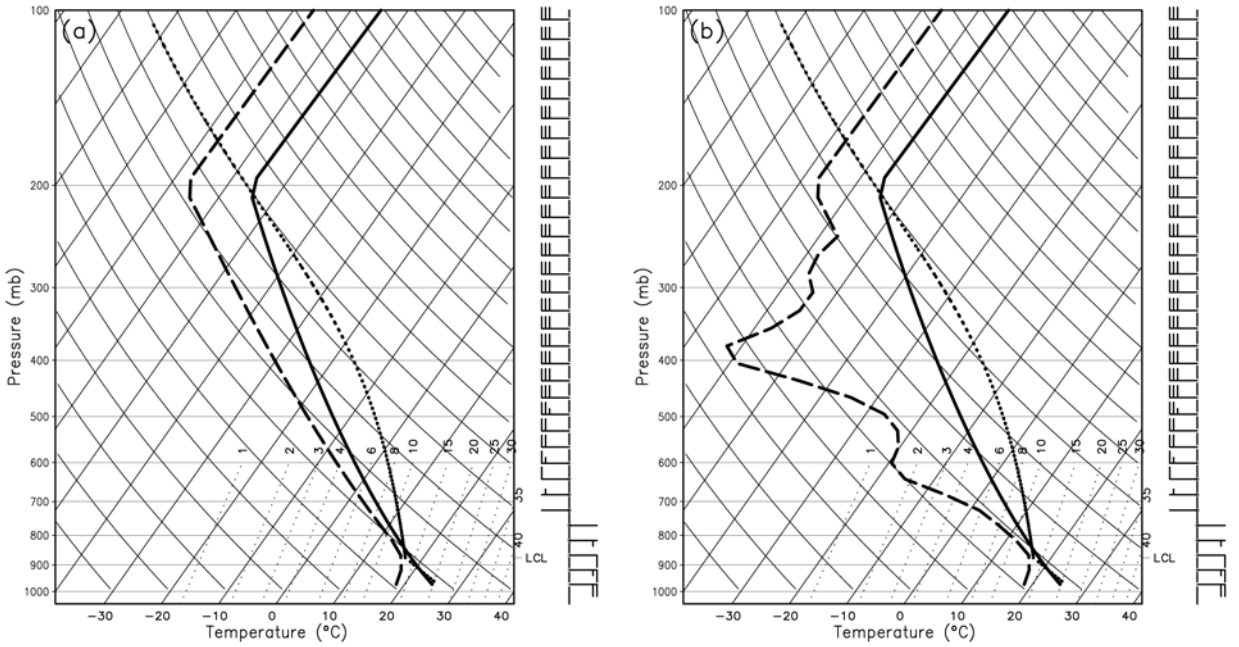

Figure 3. The base state soundings used for the two horizontally homogeneous simulations. The WK82 profile (a) represents the moist environment and (b) represents the dry midlevel environment (dry0, refer to section 2 and Table 2). The minimum RH for dry0 at 600 mb is 28% and at 400 mb is 2%. The MLCAPE for WK82 is 2079 J kg^{-1} and for dry0 is 2141 J kg^{-1} (differences arising because of the virtual temperature correction).

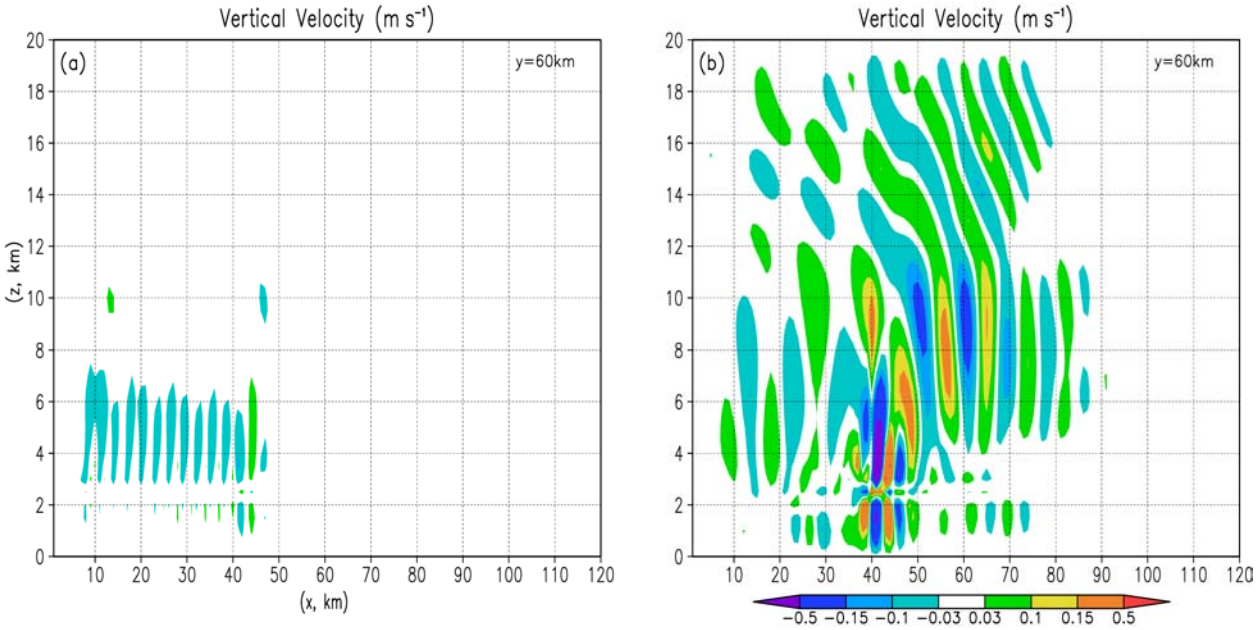

Figure 4. Horizontal cross sections of vertical velocity (m s^{-1}) at 180 min without an initial thermal perturbation for (a) the dry3 experiment as in Table 2 and Fig. 2c and (b) the dry3 experiment except using only the dry0 and WK82 soundings, separated at the x = 42 km grid location (i.e., green line in Fig. 2c). The cross sections were taken in a zonal orientation at y = 60 km.

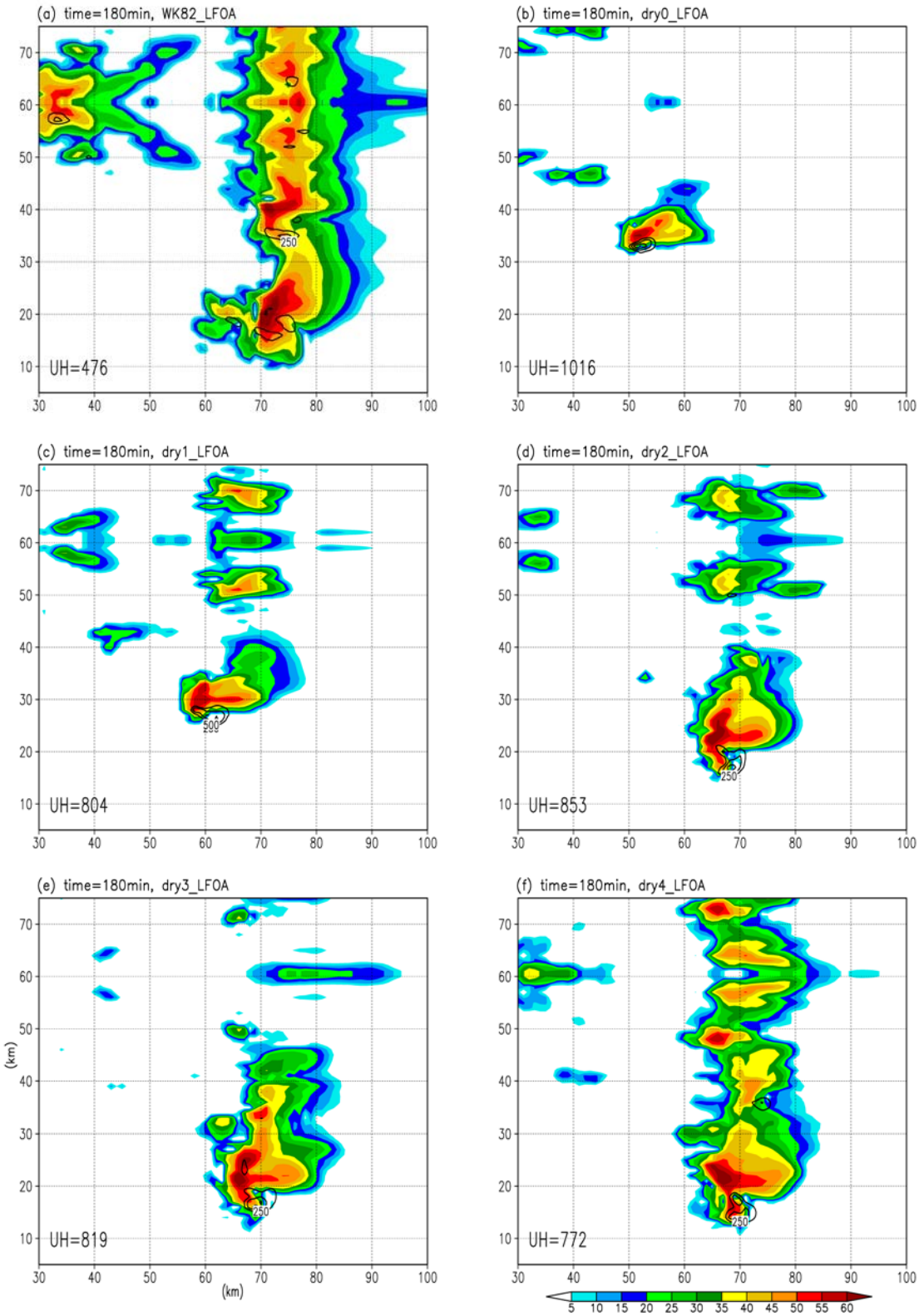

Figure 5. Simulated reflectivity at 1 km AGL (dBZ) and updraft-helicity (UH, Kain et al. 2008) from 2–5 km AGL (m^2 s^{-2}) at 180 min for the first six experiments listed in Table 2 (a–f). The LFOA microphysics scheme was used for these simulations (refer to section 2 and Table 1). The maximum UH value for the southernmost supercell is given in the lower-left corner of each panel.

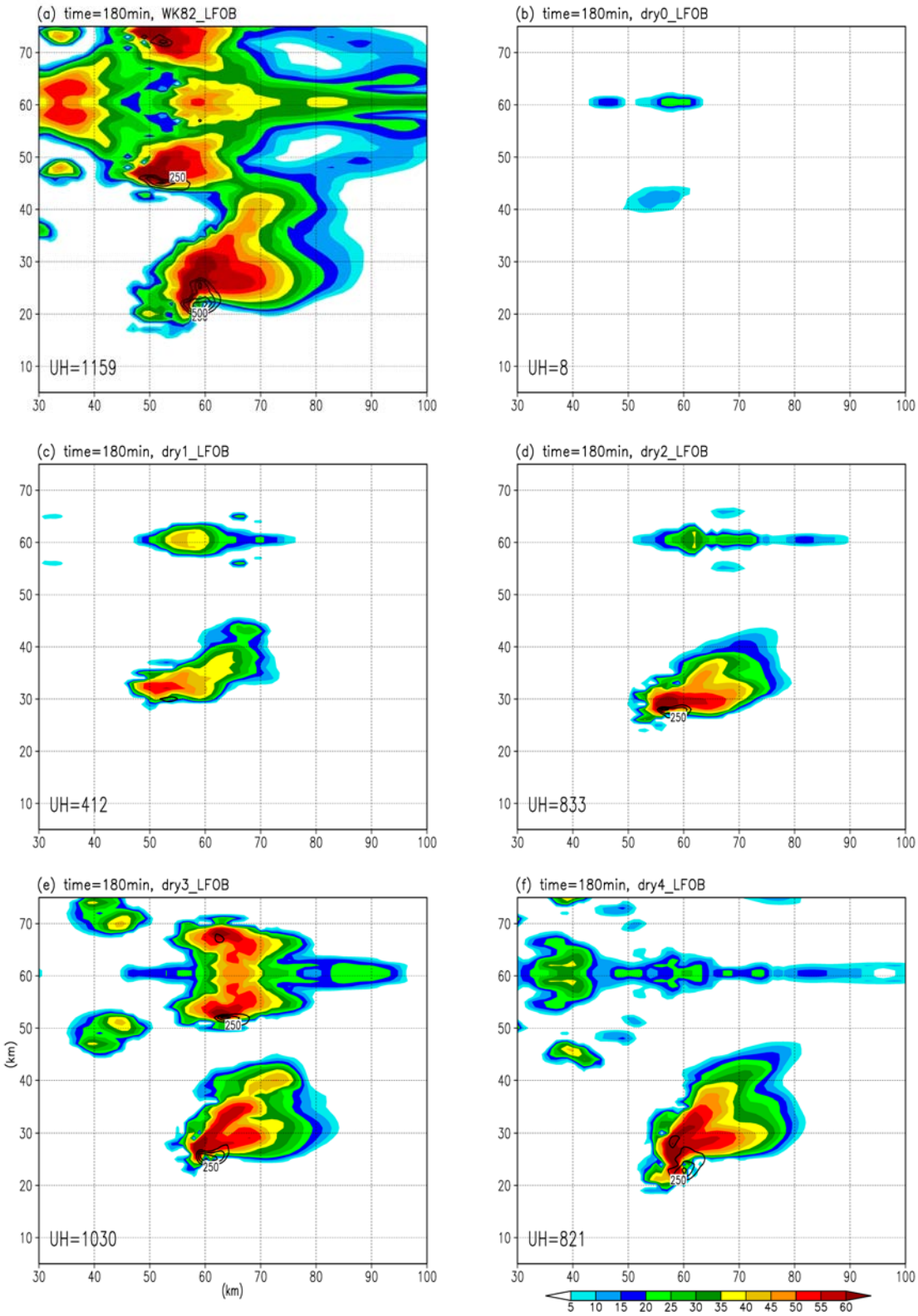

Figure 6. Same as Fig. 5 except for the LFOB microphysics scheme.

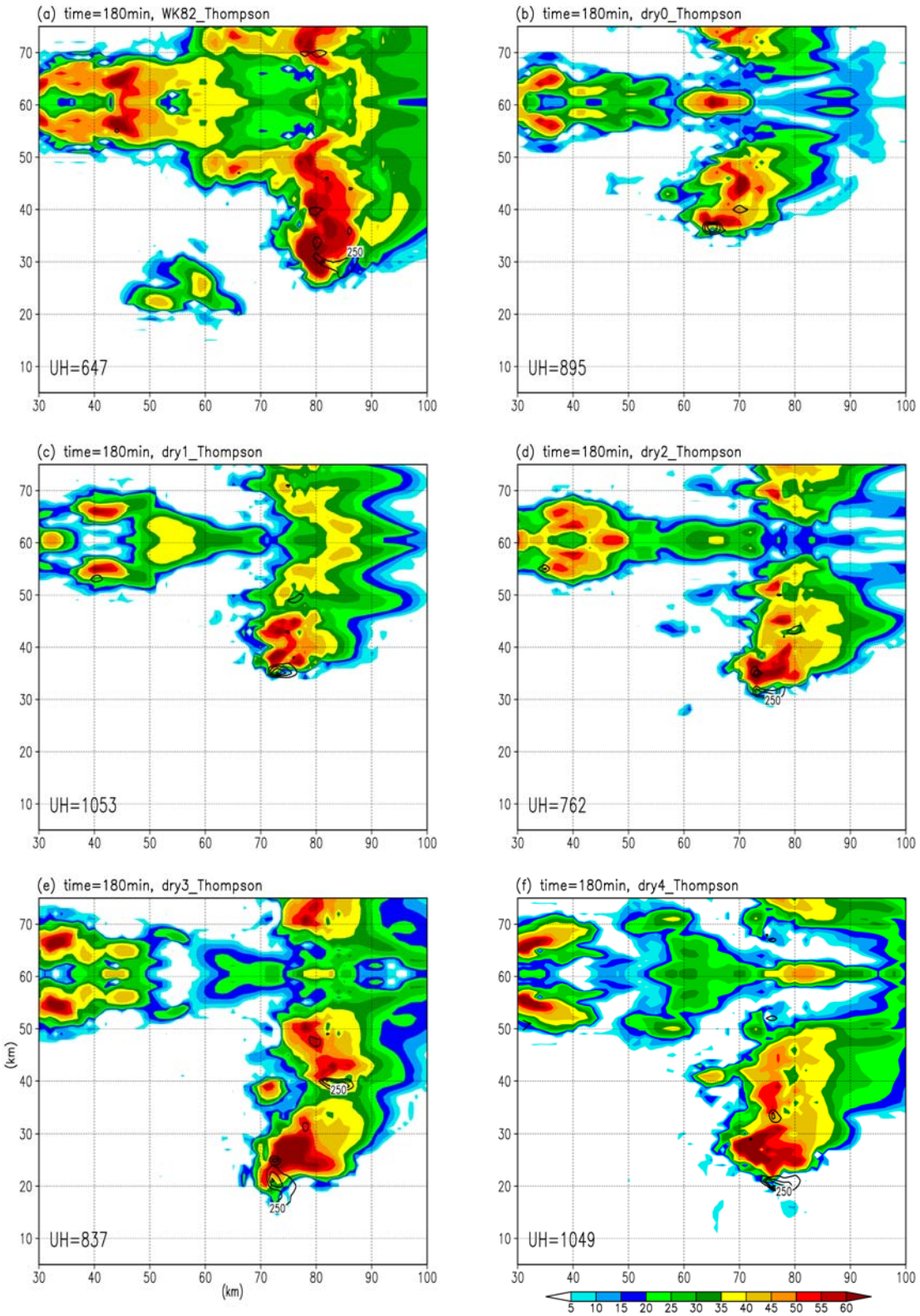

Figure 7. Same as Fig. 5 except for the Thompson microphysics scheme.

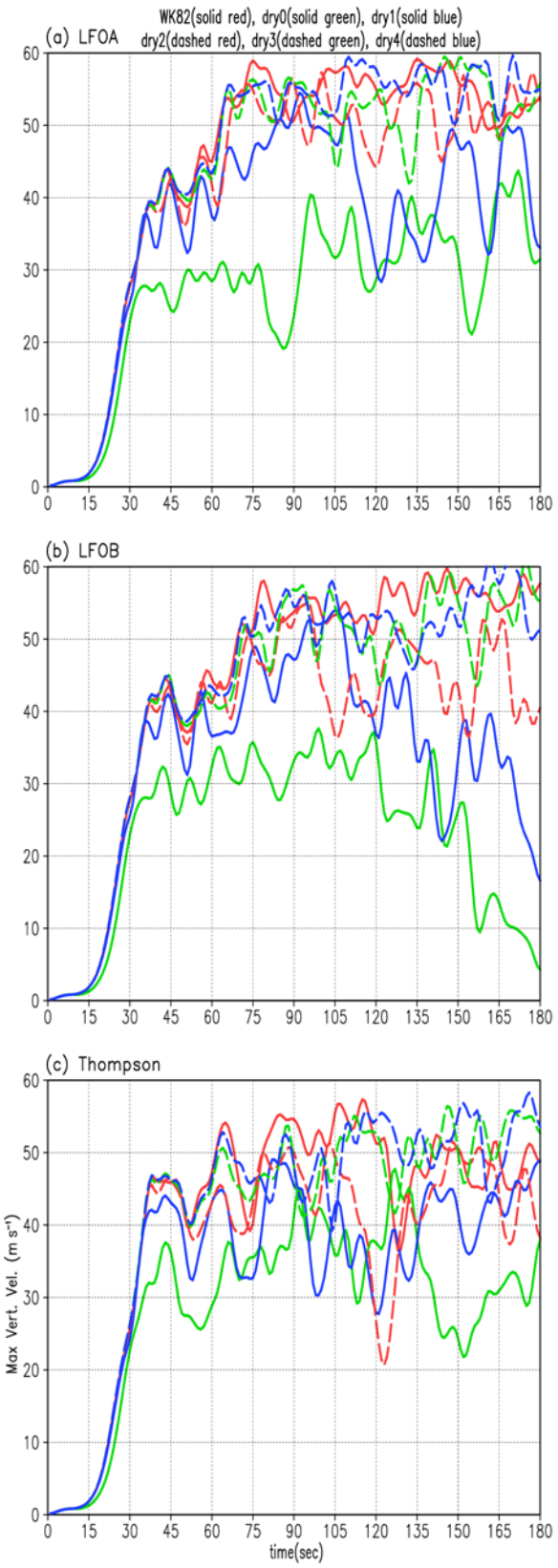

Figure 8. Time series of domain maximum vertical velocity (w_{max}, m s^{-1}) for the first six experiments listed in Table 2 (a–f) using the (a) LFOA, (b) LFOB, and (c) Thompson microphysics schemes.

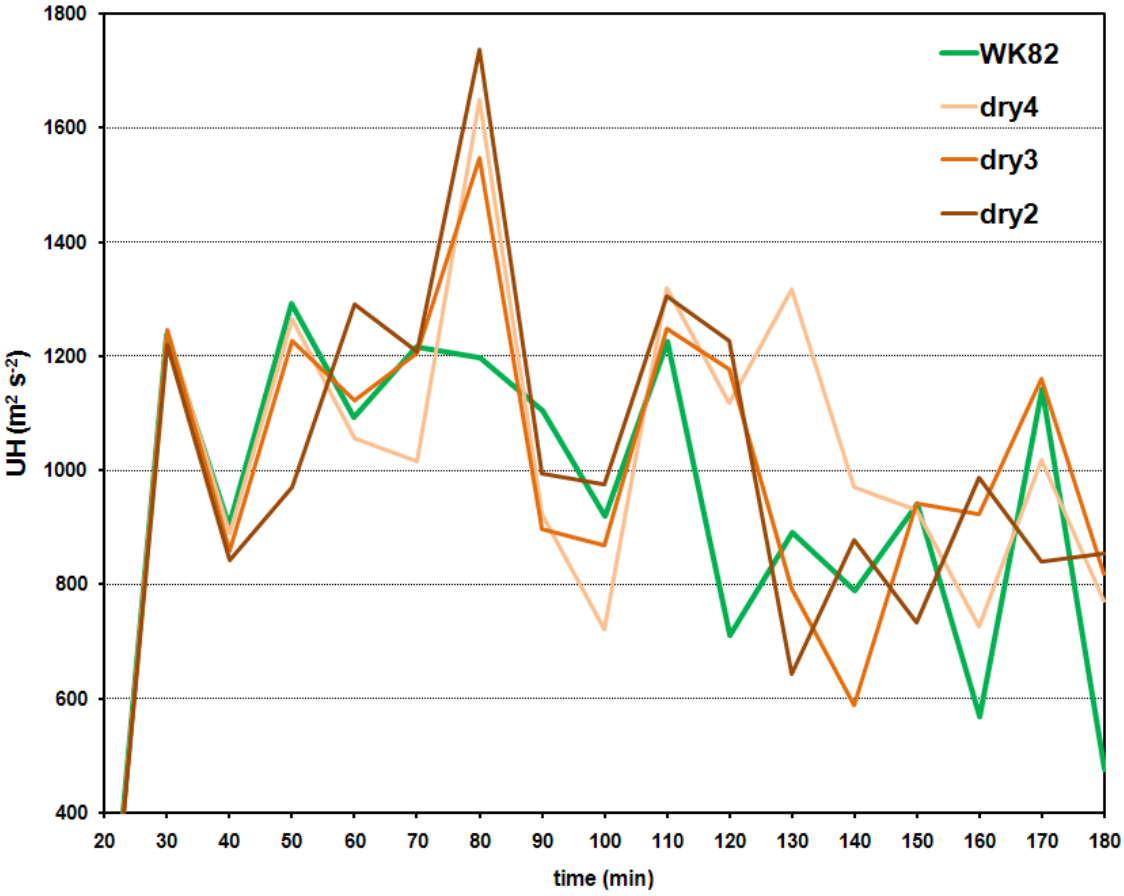

Figure 9. Time series of the maximum UH for the (a) and (d)–(f) supercell cases in Fig. 5 (for the LFOA microphysics).

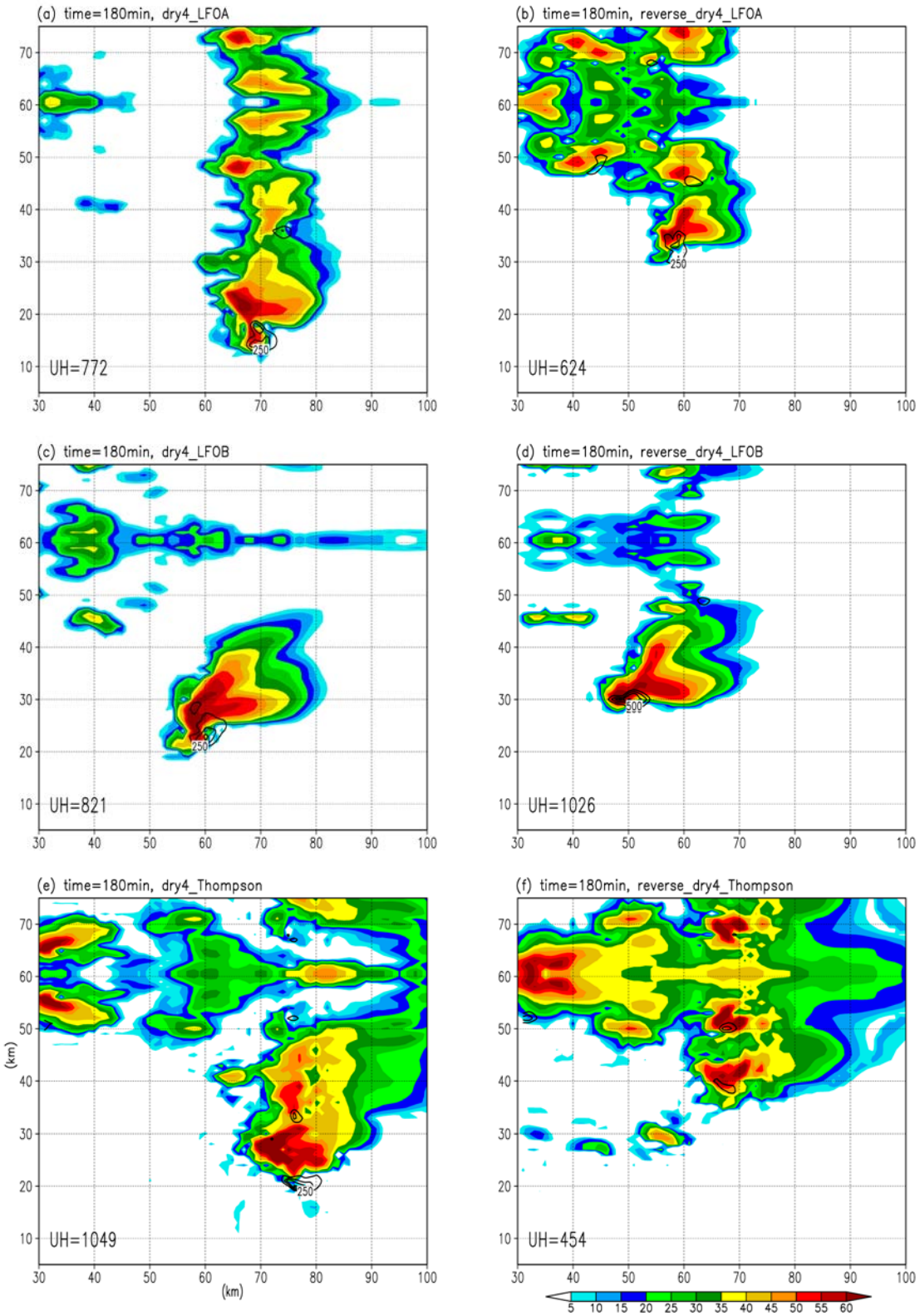

Figure 10. Same as Fig. 5 except for the dry4 (left) versus reverse-dry4 (right) simulations. The microphysics schemes are LFOA for (a) and (b), LFOB for (c) and (d), and Thompson for (e) and (f).

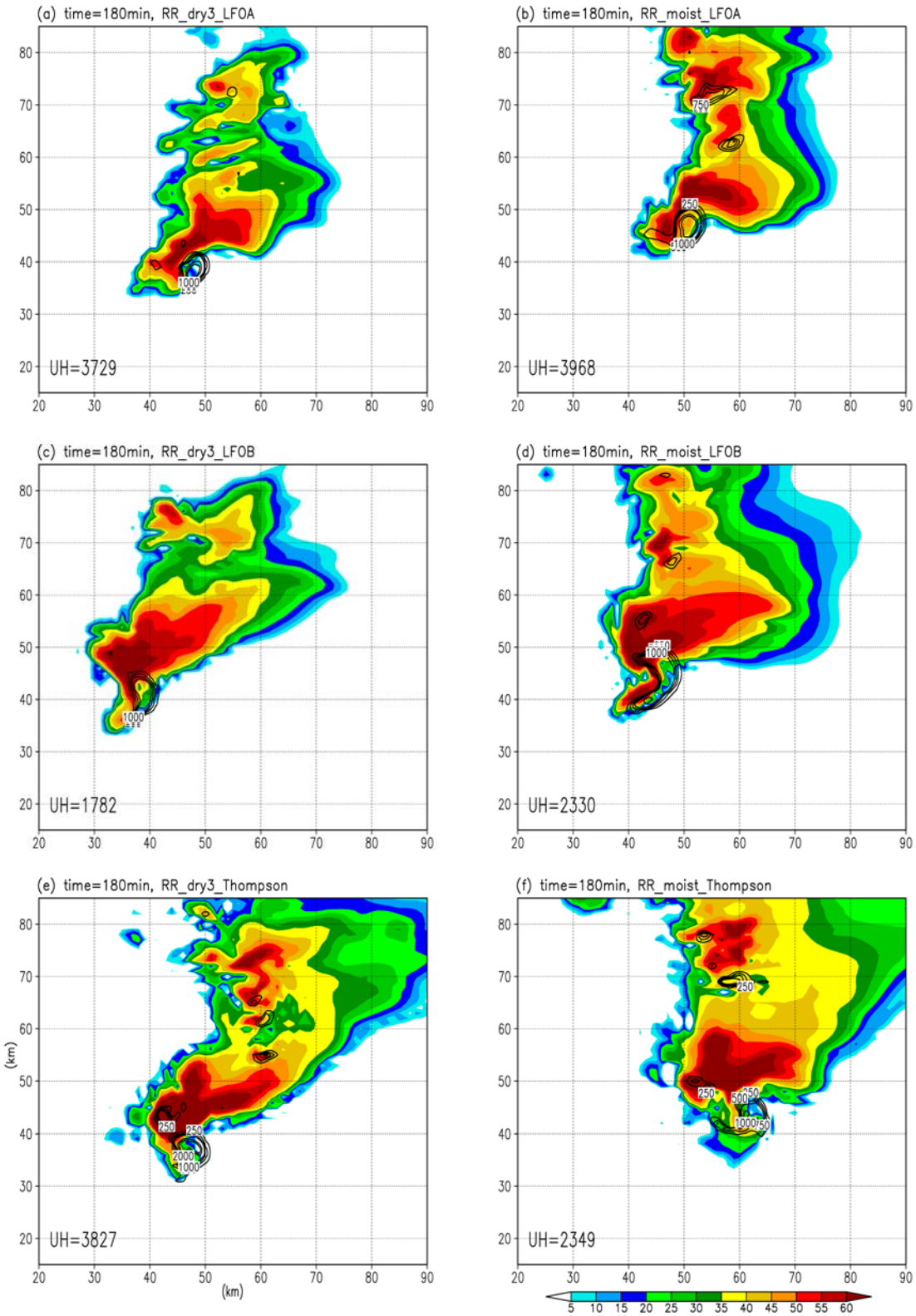

Figure 11. Same as Fig. 5 except for the simulations using the observed Red Rock and "moist" Red Rock soundings (section 3.2b) to create the horizontal moisture gradient for dry3 (left) versus the "moist" Red Rock homogeneous simulations (right). The sounding for the moist simulation had an RH = 80% above the LFC. The microphysics schemes are LFOA for (a) and (b), LFOB for (c) and (d), and Thompson for (e) and (f).